FTIR Studies of Annealing Processes in Low Temperature Pure and Mixed Amorphous Ice Samples

2 **AUTHORS**, INCLUDING:

A. Loewenschuss

Hebrew University of Jerusalem

83 PUBLICATIONS   **1,405** CITATIONS

FTIR Studies of Annealing Processes in Low Temperature Pure and Mixed Amorphous Ice Samples

A. Givan and A. Loewenschuss*,[†]

Department of Inorganic and Analytical Chemistry, The Hebrew University of Jerusalem, Jerusalem 91904, Israel

C. J. Nielsen

Department of Chemistry, University of Oslo, Blindern, N-0315 Oslo, Norway

Received: March 21, 1997; In Final Form: May 21, 1997[⊗]

Thin ice films produced by vapor deposition upon a bare CsI window as well as upon predeposited rare-gas layers or by co-deposition with rare gases may bear similarities to ices in the stratosphere and interstellar space. It was found that infrared band peak positions, bandwidths, and integrated intensities, especially those of the coupled and decoupled OH stretching mode bands, are very sensitive to structural modifications in the solid ice layers. Abrupt changes in the temperature-dependent curves of these parameters signify processes such as annealing, morphological changes, phase transitions, release of internal gas inclusions and of externally adsorbed gases, and ice grain ejection. It was shown that $(H_2O)_{as}$ annealing is a gradual process taking place even at very low temperatures. Spectroscopic similarities exist between the bulk porous ice formed by rare gas release and supercooled water solid and both differ significantly in their infrared spectra from the usual vapor-deposited amorphous ices.

Introduction

Water vapors deposited on a cold tip at low temperatures produce a metastable amorphous solid, believed to be a major constituent of interstellar[1−4] and stratospheric[5] ices. Gradual annealing to 140 and 160 K results in the transition of these amorphous layers to the better defined cubic, Ic, and hexagonal, Ih, crystalline ice forms, respectively. Reports of structural, morphological, density, surface area, and vapor pressure studies on the amorphous ice $((H_2O)_{as})$ layers indicated a large distribution of their physical properties, depending primarily upon the deposition conditions.[6−8] Under most experimental conditions a "low-density" form ($\rho = 0.94$ g/cm³) was produced. Almost the same value was suggested for the crystalline Ic and Ih ices.[6] The formation of a second high-density polymorph ($\rho = 1.1$ g/cm³[9]), distinguishable by its X-ray diffraction pattern, was shown to be dependent on a nucleation step.[10] Compared to the crystalline forms, the amorphous low-density ices show a larger dispersion of O−O bond lengths and O−O−O angle values.

Mayer et al.[8] reported that deposition of water vapors using supersonic flow conditions, as well as co-deposition of vapors and rare gases, facilitated the formation of H_2O clusters and resulted in rugged, microporous, nontransparent solids. On the other hand, slow monomeric deposition produced a transparent, nonporous, glassy ice.

Reported values of the measured surface area of the low-density amorphous ice also show considerable diversity, ranging from a few m²/g to several hundreds of m²/g.[11−14] Similarly, the existence of two or three different phases in the $T < 143$ K temperature range has been suggested.[15−17]

An extensive experimental (infrared) and theoretical study by Devlin, Buch et al.[18−25] claimed that amorphous ice, vapor deposited at $T < 90$ K, to always be microporous. Its micropores contain certain amounts of free dangling OH bonds,

responsible for the absorption of gases on the ice surfaces. A study of amorphous ice densities and refractive indices[5] as well as other low-temperature ice dynamics investigations[16,17] concluded that these physical quantities decrease either by lowering the deposition temperature or by increasing the vapor flux, attributing very low densities (0.65 to 0.19 g/cm³) and even a fluffy or needlelike morphology to these solids. Hessinger et al.[26] argued recently that shear modulus and internal friction measurements indicate the porous nature of vapor-deposited ice, which increases with lower deposition temperatures, to reach the value of 60% for a deposition at 50 K.

In a recent publication,[27] we demonstrated by infrared spectroscopy that layers formed from water vapors deposited at 5 K can form a smooth, nonporous solid that shows no absorbing capacity for CO molecules, neither when sprayed on nor when warmed after deposition. However, co-deposition of the H_2O vapors and rare gases (especially Ne), followed by warming of the sample to vaporize at least part of the rare gas, resulted in ice with surface and bulk porosity, admitting the absorption of significant CO quantities, which in turn were released completely only upon crystallization at 160 K.

Annealing processes near the crystallization temperatures were argued to be a continuous process[7] commencing already at very low temperatures.[15−17] The present study is concerned with structural annealing effects in pure and rare gas mixed deposited ices at these low temperatures, as reflected in their infrared band parameters. As during the freezing of a mixture of H_2O with the above-mentioned gases, a significant part of the guest is deposited as a separate layer,[15−17] the annealing process of double layers of (H_2O + Ar) and (H_2O + Ne) was also investigated. Spectral similarities are shown between amorphous ices of bulk porosity, from which rare gas atoms were released, on one hand, and vitrified supercooled water,[28,29] on the other.
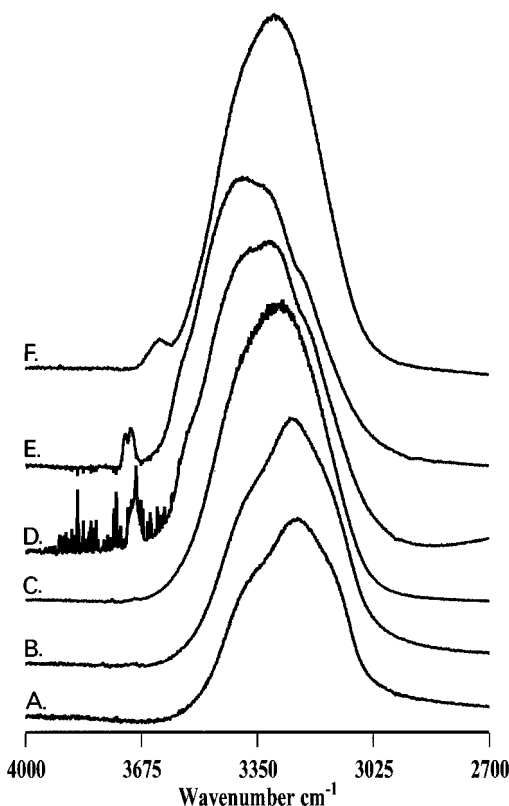
Experimental Section

Vapors of water, previously deionized and thoroughly degassed, or their mixtures with rare gases supplied by AGA, Ar

---

Pure and Mixed Amorphous Ice Samples
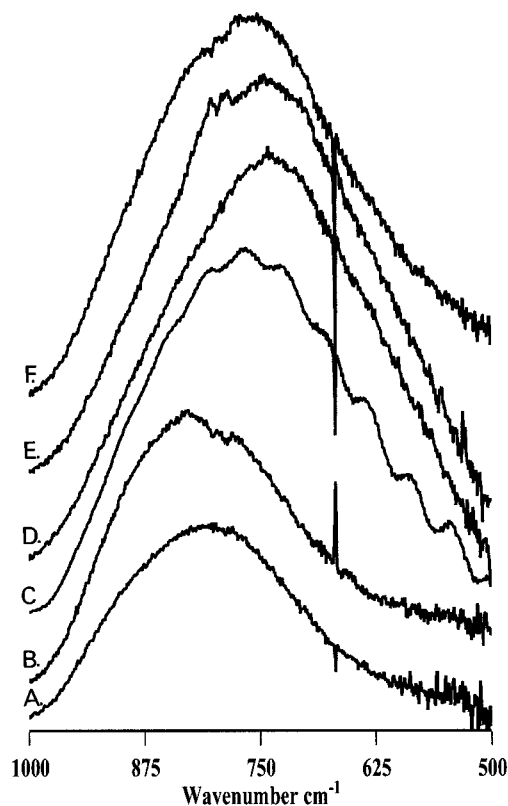
J. Phys. Chem. B, Vol. 101, No. 43, 1997 **8697**

Figure 1. ν_{OH} ("3 μm") bands of ice layers as deposited at 5 K: (A) Pure ice deposited on a CsI window. (B) Pure ice deposited on a Ne layer. (C) Pure ice deposited on an Ar layer. (D) An ice deposited from a 3:1 Ar/H$_2$O gas mixture. (E) An ice deposited from a 4:1 Ne/H$_2$O gas mixture on a CsI window. (F) An ice deposited from a 1:10 CO/H$_2$O gas mixture on a CsI window

Figure 2. ν_R bands of ice layers as deposited at 5 K: (A) Pure ice deposited on a CsI window. (B) Pure ice deposited on a Ne layer. (C) Pure ice deposited on an Ar layer. (D) An ice deposited from a 3:1 Ar/H$_2$O gas mixture. (E) An ice deposited from a 4:1 Ne/H$_2$O gas mixture on a CsI window. (F) An ice deposited from a 1:10 CO/H$_2$O gas mixture on a CsI window

(purity 5.7) or Ne (purity 4.5), were sprayed on a Kel-F-coated CsI window maintained at 5 K by an Air Products HS-4 Heliplex cryostat employing two HC-4 MK1 compressor modules. Temperature control was facilitated by a Lakeshore Model 330 temperature controller using Si diode sensors. Typical deposition rates were a few mmol/hr and the thickness of the layers was less than 0.5 μm. The deposition nozzle parameters were 1 mm inner diameter and a distance of 30 mm from the cold window. The warming rates of the investigated layers were <1 K/min. Infrared spectra were recorded on a Bruker IFS-88 interferometer equipped with a DTGS detector, with 32–128 superimposed scans and resolutions of 0.5–2 cm^{-1}.

Results and Discussion

(A) Annealing of Amorphous Ices. The low-temperature annealing stages of the following ice samples (all deposited at 5 K) will be described: (1) pure ice deposited on a CsI window; (2) pure ice deposited on a Ne layer; (3) pure ice deposited on an Ar layer; (4) an ice deposited from a 3:1 Ar/H$_2$O gas mixture on a CsI window; (5) an ice deposited from a 4:1 Ne/H$_2$O gas mixture on a CsI window; (6) An ice deposited from a 1:10 CO/H$_2$O gas mixture on a CsI window.

(A1) Infrared Spectra of 5 K Deposited Samples. The infrared spectra of all samples recorded as deposited at 5 K are shown in Figures 1–3, and the spectral data are summarized in Table 1 together with relevant data from previous studies.[7,30,31] The deposition rate of 1–2 mmol/h is sufficient to form a monomolecular layer per second. The layer thickness of about 0.5 μm, is in the range (<1.5 μm) in which the samples are still homogeneous,[7] as due to the high heat of sublimation of water ($\Delta H = 48.88$ kJ/mol[32]), the calculated rate of heat release during

condensation is about 20 mW. In several spectra slight differences in purging efficiency between reference and sample spectra are evident as residual atmospheric gas-phase lines.

The O–H stretch frequency range, briefly considered[27] in relation to the porosity of the ice layers, will be discussed here in greater detail. In the "free" OH region ($\nu > 3600$ cm^{-1}), at most two bands can be detected, and even this only for ices formed from vapors premixed with Ar or Ne (Table 1 and Figure 1D,E). These bands are rather narrow (10–20 cm^{-1}), as expected for more localized vibrational modes and have been attributed to 2- (higher frequency mode) and 3-coordinated (lower frequency mode) dangling OH bonds.[20,31]

Only insignificant amounts of these species (integrated absorption of 0.05% of the main "3 μm" band) were found in the pure ice deposited on Ar or Ne layers (Figure 1B,C) even though the enthalpy released during H$_2$O condensation is considerably higher than the cohesive energies of solid Ar or Ne (7.74 and 1.92 kJ/mol, respectively[33]). The pure ice sample deposited on a bare CsI window (Figure 1A) did not reveal these bands above noise level at all.[27] The 3623 cm^{-1} band detected in the 1:10 CO in H$_2$O sample (Figure 1F) has previously been discussed in terms of CO·H$_2$O species[27,34] and, again, is not evidence for the existence of dangling or free OH bonds in these samples.

The intense, broad coupled ν_{OH} stretching mode band of (H$_2$O)$_{as}$ shows substructures of three components in the infrared and four components in the parallel Raman spectrum. Hardin et al.[30] attributed the infrared subcomponents (in order of increasing frequency) to ν_1, ν_3, and $\nu_1 + \nu_t$ (ν_t is a lattice translational mode). According to Whalley,[35] the four Raman components are assigned to the ν_1 in phase vibration, $\nu_3 + $ TO, $\nu_3 + $ LO, and ν_1 out-of-phase modes, in order of increasing

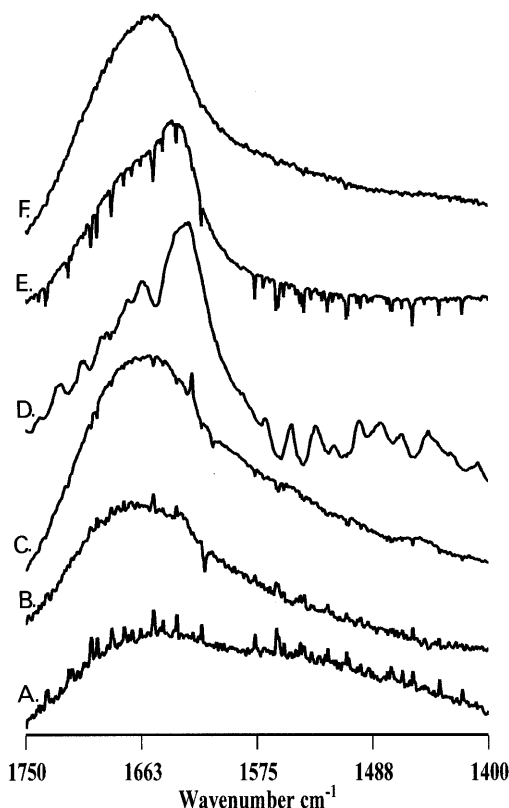**8698** *J. Phys. Chem. B, Vol. 101, No. 43, 1997*

Givan et al.

Figure 3. ν_2 bands of ice layers as deposited at 5 K: (A) Pure ice deposited on a CsI window. (B) Pure ice deposited on a Ne layer. (C) Pure ice deposited on an Ar layer. (D) An ice deposited from a 3:1 Ar/H$_2$O gas mixture. (E) An ice deposited from a 4:1 Ne/H$_2$O gas mixture on a CsI window. (F) An ice deposited from a 1:10 CO/H$_2$O gas mixture on a CsI window

frequency. Considering the complete breaking of selection rules in an amorphous sample, Rice et al.[36,37] claimed that the most correct description is to assign the lowest frequency component, at about 3100 cm^{-1}, to a vibration of ν_1 character, and the most intense infrared component, at 3250 cm^{-1}, to a mode of ν_3 characteristics. In general, considering the band as representing a density of vibrational states multiplied by their intensity function, the vibrations of maximum infrared intensity are those in which the molecules vibrate in modes correlated (as much as the structural disorder allows) with their dipole orientations, whereas maximum Raman intensity occurs when the molecules all move in phase.

The shapes of the "3 μm" (coupled ν_{OH} band, Figure 1) are different for the various layer samples investigated and must reflect their structural differences: the pure ices deposited directly on the CsI window (Figure 1A) and on a solid Ne layer (Figure 1B) show a clear three component band shape in contrast to the broad, structureless, and almost symmetrical band for pure ice deposited on an Ar layer (Figure 1C). The phonon bath of the predeposited Ar layer with its higher (than Ne) thermal conductivity[38] is more effective in removing the condensation heat of water, thus inducing the formation of the most amorphous layer of the pure ices. That the character of the bands in Figure 1A,B is more crystalline is supported by the better resolved three-component structure of the ν_{OH} absorption of ice deposited on the CsI window. Also its band peak is the closest in position to those of Ic ice infrared wavenumber of 3206 cm^{-1} [7] or the 3220 cm^{-1} Raman band.[35]

Of the three ices from premixed samples, the Ne/H$_2$O (Figure 1D) and Ar/H$_2$O (Figure 1E) bands show four partly resolved components, while the 1:10 CO/H$_2$O (Figure 1F) ice demonstrates an unresolved "amorphous" band shape. It is quite certain that a considerable amount of the added gases is deposited as an external layer.[15,27] The internal gas atoms interfere with the H-bonding between water molecules, the largest such effect being from Ne atoms, which have the highest penetration capability. The degree of this interference is evidenced by both the magnitude of the blue-shift of the "3 μm" band (Table 1) and the porosity of the ice formed upon temperature cycling of these layers.[27]

The differences in the bandwidths of the "3 μm" bands shown in Figure 1 and summarized in Table 1 are not large but significant, as they represent a measure of increase in the dispersion of bond lengths, angles, and force constants and a decrease of the intermolecular coupling. Thus $\Delta\nu_{1/2}$ decreases from the 3:1 Ar/H$_2$O ice to the 4:1 Ne/H$_2$O ice, to pure ice on CsI, to pure ice on Ne, to pure ice on Ar to the 1:10 CO/H$_2$O layer. For comparison, the bandwidth of crystalline Ic ice is 142 cm^{-1} at 10 K and 183 cm^{-1} at 140 K.[7] The peaking of this quantity in the Ar and Ne ice mixtures may be related to their clusterlike nature.[8] A very slight narrowing upon going from pure ice on CsI to one sprayed onto Ar or Ne layers, may be related to the slightly higher temperature sensed by the H$_2$O vapors deposited on the latter. The lowest bandwidth (318 cm^{-1}) is that of the ice formed from a 1:10 CO/H$_2$O mixture ice. In this sample with only a few percent of CO in the ice lattice, H$_2$O condenses around small CO clusters (27, 34) which fulfill the role of nucleation grains.

The spectrum of pure ice (Figure 1A) was subtracted from each of the other five spectra. The results emphasize resemblance of the pure ice spectrum to its parallel on Ne layer. In the pure ice on an Ar layer, the difference spectrum shows bands at 3313 and 3439 cm^{-1}. For the Ar and Ne ice mixtures, the difference spectra have features in the 3300, 3450, and 3550 cm^{-1} regions. Samples with high guest concentrations show more high-frequency oscillators (3450 and 3550 cm^{-1}), attributed to less coupled, more localized OH stretching modes. The 3550 cm^{-1} frequency is close to that of several OH containing solids, e.g., hydroxyapatite[39] (3571 cm^{-1}). Even though LO−TO splittings in disordered materials as vitreous silica and germania are known to have been observed,[40] the high concentration found here of Ar/Ne guest molecules is expected to strongly minimize this mode coupling. Thus, the increase of the 3300 and 3450 cm^{-1} bands speaks against their assignments to $\nu_1 + \nu_t$[30] or to $\nu_3 +$ LO[35] and supports the more general one by Rice et al.[36,37] Similar results are obtained by curve-fitting calculations. In addition, these procedures emphasize the existence of a low-frequency component around 3150 cm^{-1} also in the mixed ice samples. This frequency, which has a Raman parallel at 3116 cm^{-1},[41] is attributed[7,30,35−37] to the ν_1 symmetric stretch mode. Whalley[35] assigns this band to intermolecularly coupled ν_1 in phase vibrations in clusters of at least 25 molecules. If this is indeed the case, our mixed ices may contain such clusters.

The intermolecular rotational ν_R region of all samples is reproduced in Figure 2 and summarized in Table 1. Here, again, ν_R bands are narrower for the pure ices on bare CsI and on solid Ne layers and for the 1:10 CO/H$_2$O mixed ice layer, the samples argued above to be of a more crystalline nature. Difference spectra and band deconvolution calculations show that the shifts and widths of the ν_R bands of the other samples, relative to the pure ice on CsI one (peaking at 798 cm^{-1}), is due to the growing in of a low-frequency component at $\nu <$ 670 cm^{-1} in addition to the existence of a high-frequency one at $\nu >$ 850 cm^{-1} (in analogy to hydroxyapatites, where the emergence of a 630 cm^{-1} band accompanies the growth of the 3570 cm^{-1} band[39]). We attribute the former to smaller water

TABLE 1: Frequency Positions (cm^{-1}) and Width at Half Intensity (cm^{-1}) of Infrared Bands of Pure and Mixed Ice Layers as Deposited at 5 K

ice layer	ν_{OH}	$\Delta\nu_{1/2}$	ν_2	$\Delta\nu_{1/2}$	ν_R	$\Delta\nu_{1/2}$
pure ice deposited upon a CsI window	3390(sh); 3234; 3140(sh)	330	1653; 1550(sh)	367[a]	798	206
pure ice deposited upon a neon layer	3390(sh); 3257; 3150(sh)	325	1653	98	827; 770(sh)	187
pure ice deposited upon an argon layer	3390(sh); 3276	322	1656; 1560(sh)	129	765	210
3:1 Ar/H$_2$O mixture deposited upon a CsI window	3695; 3550(sh); 3420(sh); 3310; 3210(sh)	345	1660(sh); 1635	88	740	262
4:1 Ne/H$_2$O mixture deposited upon a CsI window	3704; 3720; 3570(sh); 3390; 3300(sh); 3220(sh)	343	1680(sh); 1639	78	745	270
1:10 CO/H$_2$O mixture deposited upon a CsI window	3623; 3300	318	1640(sh); 1657	87	824(sh); 737	193
pure ice, ref 7	3402(sh); 3257	310	1665			
pure ice, ref 30	3367(sh); 3253; 3190(sh)	322	1660; 1570(sh)	350	846(sh); 802; 675(sh)	220
Ar/H$_2$O mixture, ref 31	3650		1640; 1550(sh)		765; 650(sh)	

[a] Total bandwidth (both components).

clusters and the latter to the disrupting effect of guest molecules on the H-bond system.

In the discussion of the band originating in the coupled ν_2 bending modes in the 1620−1680 cm^{-1} region, their proximity to the $2\nu_R$ frequency values has to be considered.[30,35] In our spectra for this region, reproduced in Figure 3 (frequencies and bandwidths listed in Table 1), it is immediately apparent that the band of the pure ice on bare CsI has a distinct low-frequency component (peaking at about 1550 cm^{-1}) which is significantly reduced in the mixed ice spectra and even in the spectrum of pure ice on predeposited rare-gas layers. The sensitivity of overtones of librational modes to disorder has been previously pointed out by us.[42] The ν_2 band of pure ice on CsI peaks at 1653 cm^{-1} and upon mixing with Ne and Ar shifts to lower frequencies (1635 and 1639 cm^{-1}, respectively), in accordance with the decrease in intermolecular coupling. On the high-energy side (1660 cm^{-1}) of the ν_2 bands of the mixed ices, the emergence of a band is noted, which can be interpreted as an overtone of the high-frequency component of its ν_R band, discussed above.

In summary, during the dilution of the H$_2$O component of the ices investigated, in addition to the 3390, 3234, 3140, 1653, 1550, and 800 cm^{-1} pure ice bands, new features appear at about 3550, 3450, 1660, 1635, 850, and 650 cm^{-1}, attributable to H$_2$O clusters of various sizes.

(A2) Annealing Experiments. (1) Pure Ice Deposited on CsI Window at 5 K. The spectral effects of annealing are demonstrated for ν_{OH} for all samples considered in Figure 4, while the changes in band parameters ν, $\Delta\nu_{1/2}$, and A, the integrated absorbance, are presented in Figures 5−7, for the temperature region 5−70 K.

In the ν_{OH} stretching mode region, the effect of warming (Figures 4A and 5A) is on the low- and high-frequency shoulders (3390 and 3140 cm^{-1}, respectively), reducing the first and increasing the latter. The band thus acquires a *gradual and irreversible* similarity to that of crystalline Ic ice.[7,27,30] However, the central peak at 3234 cm^{-1} remains, essentially, unaffected. Hardin et al.[30] warmed (H$_2$O)$_{as}$ samples in the 92−135 K range and also noted that their ν_{OH} values decreased irreversibly only in the crystallization range above 135 K. On the other hand, Hagen et al.[7] reported a slow, *continuous* decrease of the ν_{OH} peak wavenumber due to warming from 10 to 130 K. In addition we found no exceptional change at 60 K, a temperature for which Devlin et al. report[20] a drastic reduction in the amount of 2-coordinated dangling OH bonds. Thermal changes are composed of reversible thermal expansion effects[43] and irreversible annealing processes, unaffected by recooling to 5 K. Thus the lack of a significant temperature effect on ν_{OH} indicates that, in the present case, these two opposing trends approximately cancel each other. This and the

fact that ν_{OH} of our pure ice sample is about 20 cm^{-1} lower than that of Hagen et al.[7] also indicate our sample to be of a higher crystalline nature.

The annealing effect on $\Delta\nu_{1/2}$ (Figure 6A) of the ν_{OH} band is a continuous reduction of its value (4.5% from 5 to 60 K), indicating a decrease in disorder and in the *extent* of intermolecular coupling strengths.[35] Together with the increase with temperature of the low component of the band, described above, it is evidence of the growth of a strong H-bonds fraction in the solid, at the expense of the weaker bonded ones.

The integrated absorbance (A, Figure 7A) is expected to increase during annealing, due to better ordering of the oscillator dipoles. However, this parameter has a minimum at around 30 K. Thus, A is a more sensitive parameter to structural effects than ν and $\Delta\nu_{1/2}$ and so the 30 K temperature region is a clear stage in the annealing process.

The ν_2 mode band is weaker and less clearly resolved. Generally, upon annealing, its band parameters parallel those of ν_{OH}, with the weak shoulder at 1550 cm^{-1} gaining intensity to almost reach that of the main 1653 cm^{-1} component at around 60 K.

The ν_R band of a pure ice layer as deposited at 5 K is broad (206 cm^{-1}, Figure 8 and Table 1) essentially symmetrical band. Upon warming, the absorption shows a substructure on its peak which gets better resolved up to 30 K and then disappears slowly upon further warming to 60 K. Recooling to 5 K causes the reappearance of this structure. We tend to attribute this reversible phenomenon to index of refraction changes associated with rotational ordering of the ice. Up to 60 K, the peak frequency is essentially unchanged with temperatures and $\Delta\nu_{1/2}$ slightly decreases irreversibly. Due to the detector range, integrated intensities could not be determined accurately.

These observations are in accord with the external modes of ice (due to the extensive hydrogen-bonding network, translational and librational modes are essentially inseparable) being the main sources of heat capacity in ice I below 80 K[44] and that this ice also goes through a structure or order change around 30 K, as was also indicated by our considerations of the integrated intensity $A(T)$ above. Indeed, Bar-Nun et al.[17] suggested 35 K to be the first temperature at which ice annealing and not the physical properties of Ar is the main factor of its release from argon/ice premixed samples.

(2) Annealing of Pure Ice Deposited on a Ne Layer. The effects of annealing on ν_{OH} of this ice are depicted in Figure 4B and the temperature-induced changes in the parameters ν, $\Delta\nu_{1/2}$, and A values shown in Figures 5B, 6B, and 7B. The (H$_2$O)$_{as}$ and Ne layers are about 0.5 μm thick, and as pointed out above the ice is of a more homogeneous and crystalline nature, compared to the premixed ones. In the lowest annealing range, solid neon first softens to eventually evaporate at 12−
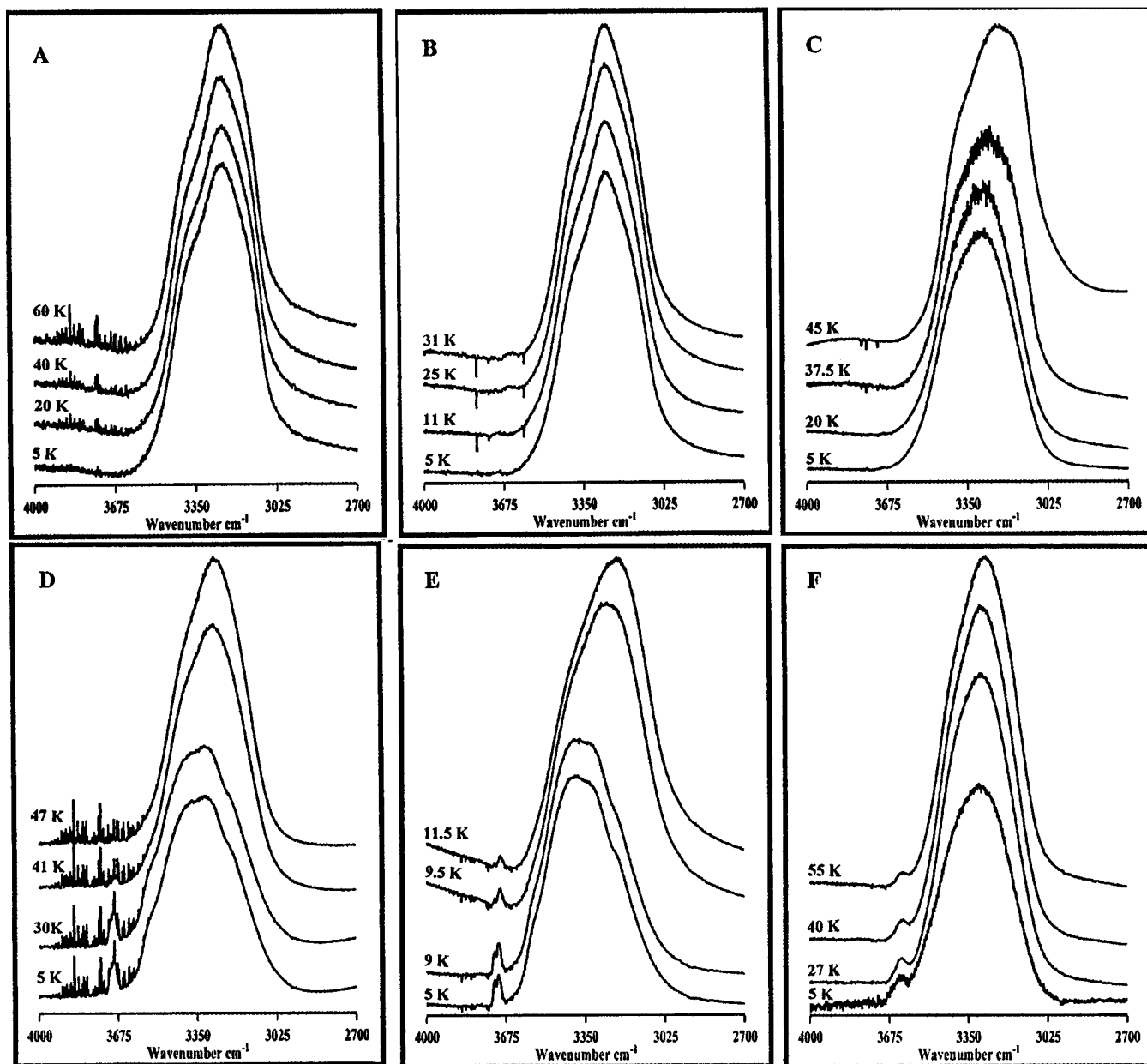
Figure 4. Annealing effects on ν_{OH} (3 μm) band of: (A) Pure ice deposited on a CsI window. (B) Pure ice deposited on a Ne layer. (C) Pure ice deposited on an Ar layer. (D) An ice deposited from a 3:1 Ar/H_2O gas mixture. (E) An ice deposited from a 4:1 Ne/H_2O gas mixture on a CsI window. (F) An ice deposited from a 1:10 CO/H_2O gas mixture on a CsI window.

13 K (noted by a system pressure increase). This destabilizes the immediate parts of the amorphous ice and implies a different, multimodal approach[8] to its structure. Spectroscopically, these changes are more apparent in the graphs showing the temperature dependence of the spectral parameters (Figures 5B, 6B, and 7B) than in the inspection of the band shapes (Figure 4B): ν_{OH} and $\Delta\nu_{1/2}$, decreasing irreversibly with temperature, show a small minimum and maximum respectively around 10 K, whereas an inflection point is noticed in the increasing $A(T)$ values. The small change in ν_{OH} again indicates that annealing slightly overcomes the thermal expansion effects. The integrated intensities (Figure 7B) indicate no ejection of ice grains along with the neon release around 10−13 K, as reported for premixed samples.[16,17] On the other hand, these values reflect, by a steep increase, the structural change at around 30 K. The band structure is similar to that found for ice deposited on a bare CsI window. The enhancement with temperature of the low-frequency component of the ν_{OH} band is also observed here, to some greater extent.

The ν_2 band parameters again follow those of ν_{OH}. Its frequency, too, is almost constant and shows a similar minimum at around 13 K as in Figure 5B. $\Delta\nu_{1/2}(T)$ decreases irreversibly with T, while $A(T)$ increases, also irreversibly, showing the inflection about 13 K seen in Figure 6B (but not the increase around 30 K). The development of the 1550 cm^{-1} shoulder with temperature noted in the pure ice on a CsI window was not observed here. The ν_R parameters show slight decreases of peak position and bandwidths with temperature, while integrated intensities could not be determined reliably.

(3) Annealing of Pure Ice Deposited on an Argon Layer. The annealing process in the ν_{OH} band of this sample is shown in the spectra of Figure 4C, and the graphs of the temperature dependences of the spectral parameters in Figures 5C, 6C, and 7C. From pressure measurements it is evident that argon release occurs at 40−45 K involving also a release of ice grains, as indicated by the sharp changes in the latter, especially the large (30%) decrease in the A values (Figure 7C), not found for the other pure ices (Figure 7A,B).
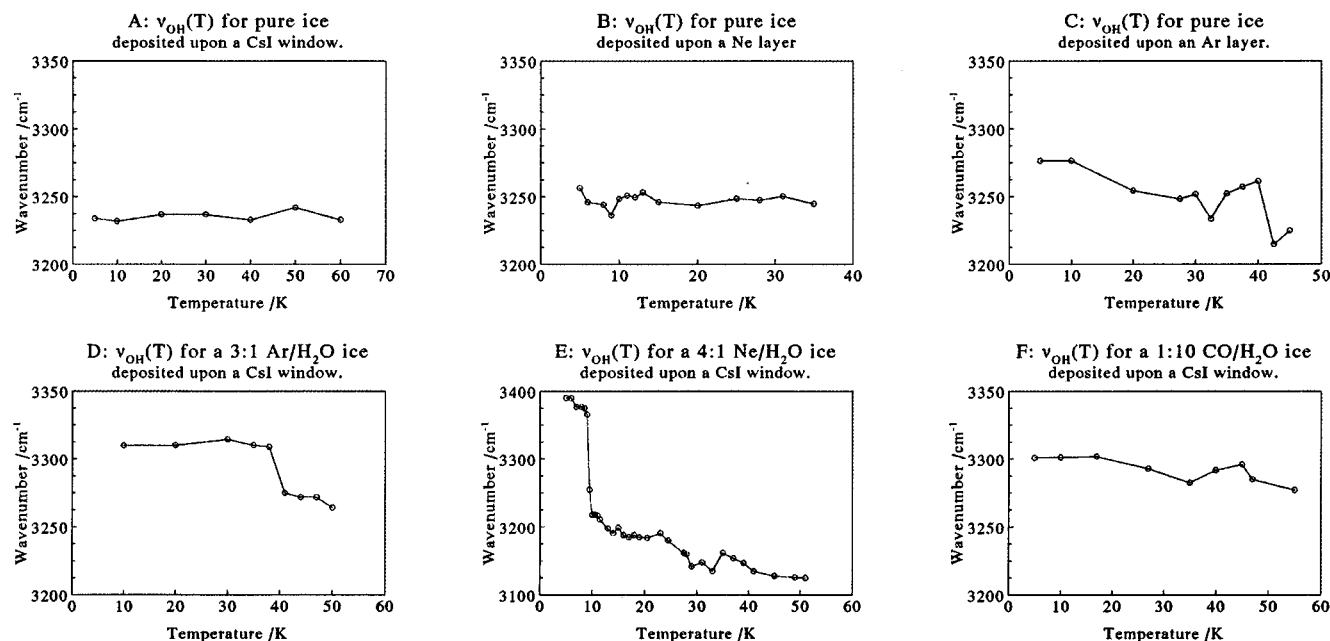
Pure and Mixed Amorphous Ice Samples

J. Phys. Chem. B, Vol. 101, No. 43, 1997 **8701**

Figure 5. Temperature dependence of wavenumber positions of ν_{OH} ("3 μm") bands of ice layers.

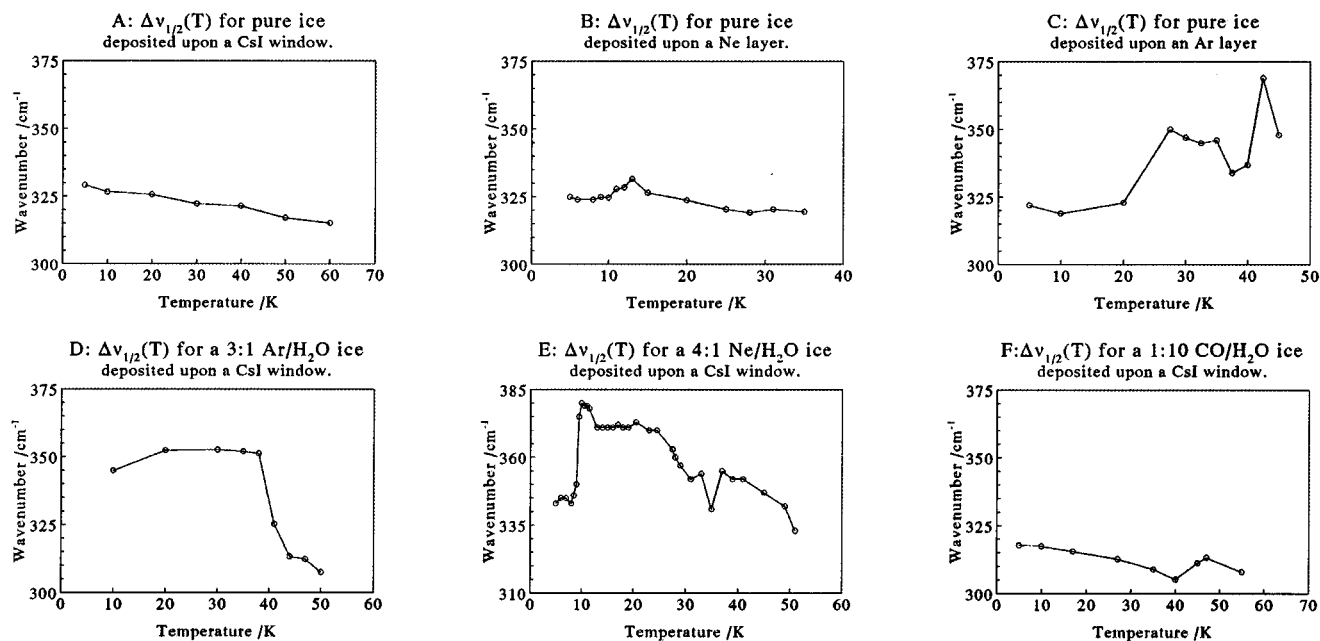**Figure 6.** Temperature dependence of bandwidth at half intensity of ν_{OH} ("3 μm") bands of ice layers.

The lack of spectral features in the $\nu > 3600$ cm^{-1} region is evidence for the scarcity of "free" dangling OH bonds, even at the argon/ice interface. The ν_{OH} peak, looks rather symmetric at 5 K, but its three component structure clearly emerges at 45 K. With increasing temperature the overall intensity is reduced and the low-frequency band constituent gains relative weight from a ratio of 4.5:5:1 (for 3410, 3270, and 3190 cm^{-1} as peak positions for the components) at 5 K to 1:1.4:1.3 at 45 K. Adopting the approach of Whalley,[35] attributing this low component to the in phase ν_1 collective mode of more than 25 molecules, argon release breaks the covering ice layer and preferentially ejects smaller H$_2$O clusters but does not increase the amount of free OH bonds.

The decreasing peak frequency (Figure 5C) shows two minima at 32 and 42 K, corresponding to the (H$_2$O)$_{as}$ annealing stage found above, and argon release, respectively. The overall red-shift of about 55 cm^{-1} in the 5–50 K range, is very different

from the constant band position found for pure ice deposited on a CsI window (Figure 5A) or the slight change found for ice on a solid Ne layer (Figure 5B) and is also consistent with the assumption that weaker bound clusters are ejected by the evaporating argon.

By taking X-ray data (on Ih ice),[43] frequency shifts were "calibrated" to indicate the temperature dependence of the oxygen–oxygen distances in amorphous ices,[7] confirming that for the small O–O separations at these very low temperatures a large $\Delta\nu/\Delta R$ slope reflects a strong stabilization of the hydrogen bonds.[45] Our observed shifts for amorphous ice on an argon layer exceed those by Hagen et al.[7] over the measured temperature range and, again, indicate a drastic decrease in the *average* O–O distance, or the expulsion of clusters with weaker bonding and longer r(O–O) values.

The two minima found in the band position of $\nu_{OH}(T)$ (Figure 5C) have corresponding maxima in the graph describing the
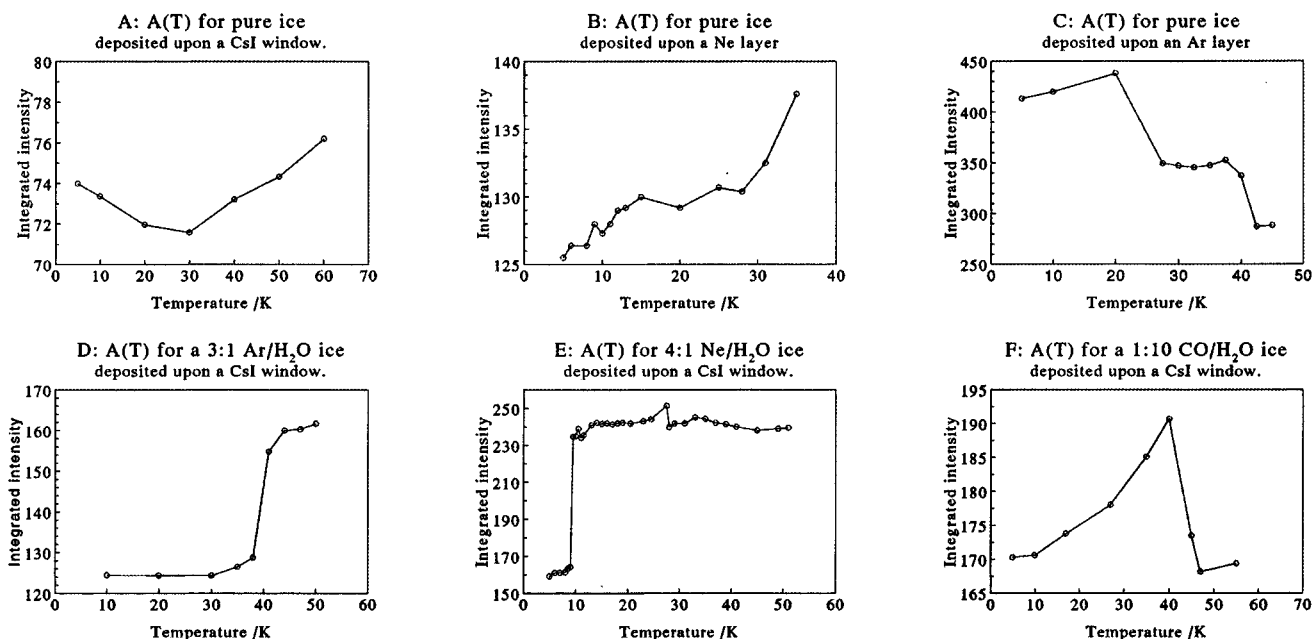
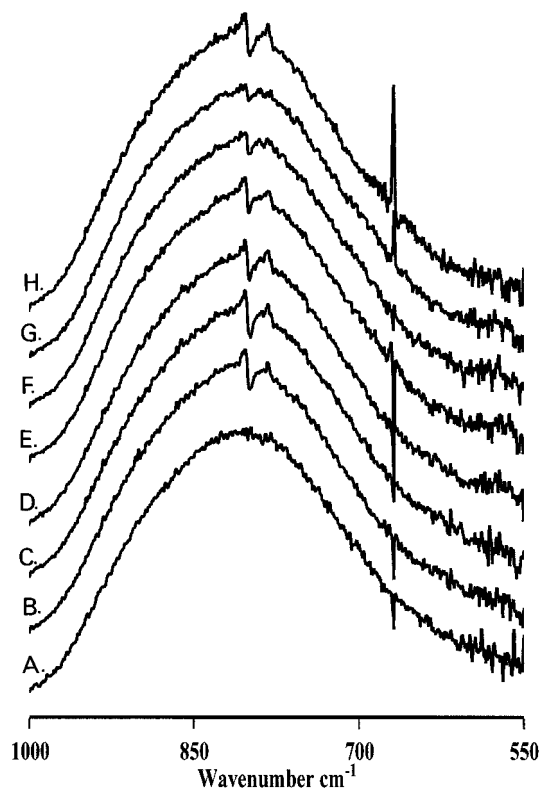**Figure 7.** Temperature dependence of integrated intensities of ν_{OH} ("3 μm") bands of ice layers.

Figure 8. Temperature induced changes in ν_R of an ice deposited on a CsI window. (A) As deposited at 5 K. (B) Warmed to 10 K. (C) Warmed to 20 K. (D) Warmed to 30 K. (E) Warmed to 40 K. (F) Warmed to 50 K. (G) Warmed to 60 K. (H) Recooled to 5 K.

temperature dependence of the ν_{OH} bandwidth (Figure 6C). Thus despite the evidence for the ejection of weaker bound clusters, discussed above, the growing bandwidths still reflect increasing disorder in the remaining ice layer, involved in major transformations, induced either by temperature or by argon evaporation. These transformations are also evidenced by the slope changes in the graph of $A(T)$ of integrated intensity versus temperature (Figure 7C), in addition to the overall decrease in its value, noted above.

The ν_2 band, as deposited at 5 K, peaks at 1656 cm^{-1} and does not reveal the 1550 cm^{-1} shoulder, typical of pure ice on

CsI. However, upon warming, this shoulder rapidly and irreversibly grows to effectively double the bandwidth at about 45 K.

The ν_R band shows a significant irreversible blue-shift, indicative of stronger H-bonding, from 765 cm^{-1} at 5 K to 816 cm^{-1} at 50 K. The $\Delta\nu_{1/2}(T)$ values reflect, by slight minima, the irreversible changes occurring in the ice layer around 30 K and 45 K emphasizing the differences with regard to pure ice on a CsI window. Again, a 30% decrease in integrated intensity, $A(T)$, is associated with the effects of argon evaporation on the layer.

(4) Annealing of a 3:1 Ar/H$_2$O Sample. The process is demonstrated in the infrared spectra of Figure 4D and the $\nu(T)$, $\Delta\nu_{1/2}(T)$ and A(T) graphs in Figures 5D, 6D, and 7D. A prominent feature in this sample, not observed in the pure ice layers, is the presence of the 3692 cm^{-1} band in the uncoupled OH region. Previously[18-25] these frequencies were attributed to dangling OH bonds, in micropores of the high surface low-temperature ice, persisting up to 120 K (where the pores collapse). We assign this band with an integrated absorption of 0.5% of the main coupled ν_{OH} absorption, to small ice clusters possessing free OH groups and dispersed in the argon matrix. This assignment is in accord with their almost complete disappearance at about 40 K, when most of the argon is released (Ar equilibrium vapor pressure is then about 0.01 Torr, 10 000 times the system vacuum).

Figure 4D shows the conversion of the four component ν_{OH} band at 5 K, discussed in section A1, to the three component band of pure ice (3400, 3280, 3180 cm^{-1}) at around 40 K. After warming and disposing of the argon, the low-frequency band components, at 3180 and 3280 cm^{-1}, gain intensity as compared to the 3400 cm^{-1} group, confirming the more clusterlike nature of the latter.

The $\nu_{OH}(T)$ graph in Figure 5D, shows an essentially constant band position up to the temperature at which the argon is released, when a drastic irreversible red shift of 45 cm^{-1} is affected. Specifically, the annealing stage at around 30 K, noted for pure ice is prevented by the presence of frozen argon in the ice layer.

When comparing the $\Delta\nu_{1/2}(T)$ graph of this sample (Figure 6D) with that for ice on a predeposited argon layer (Figure 6C), it is evident that here the increasing temperature has an opposite

Pure and Mixed Amorphous Ice Samples

J. Phys. Chem. B, Vol. 101, No. 43, 1997 **8703**
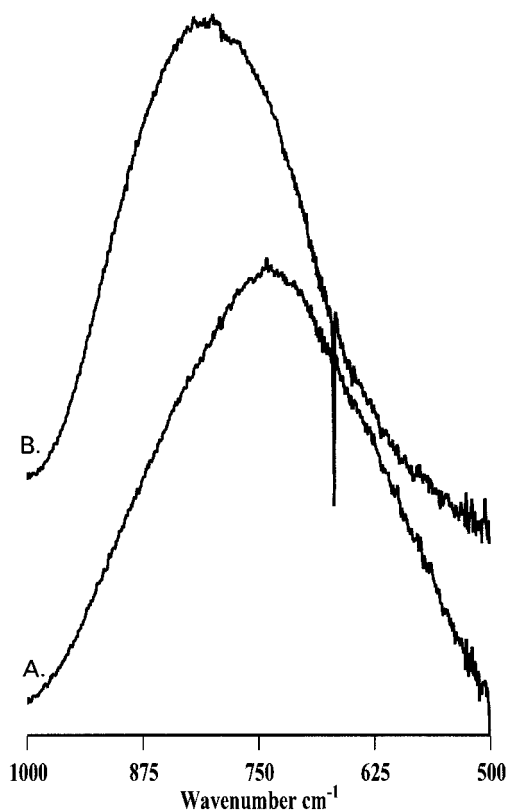
Figure 9. Temperature induced changes in ν_R of an ice deposited from a 3:1 Ar/H$_2$O gas mixture. (A) As deposited at 5 K. (B) Warmed to 50 K, recooled to 5 K.

result of *reducing* the bandwidth, this effect being most prominent around the temperature of argon release. This is, however, not surprising in view of the elimination of the high-frequency band component, discussed above.

In the $A(T)$ graph (Figure 7D), the temperature, again, has an opposite effect to that noted in Figure 7C for ice on predeposited argon. However, here the *increase* in intensity, despite the lower width and the only three component structure, is more surprising and may be rationalized by assumimg that the release of argon atoms from within the ice layer, affects a better intermolecular ordering of the H$_2$O dipoles, without necessarily ejecting weaker bounded water clusters.

In the weaker ν_2 band (1635 cm^{-1} at 5 K), an additional shoulder at 1660 cm^{-1} develops upon warming to 50 K, but its low intensity precludes a detailed discussion of it spectral parameters. On the other hand, the ν_R band data support the conclusions derived from the ν_{OH} band. Its band frequency increases significantly with temperature (from 735 cm^{-1} at 5 K (same for 8 K) to 808 cm^{-1} (50 K), Figure 9) along with a decrease in bandwidth, with the most drastic changes occurring at about 42 K, and generally following the changes of ν_{OH} (Figures 5D and 6D).

(5) Annealing of a 4:1 Ne/H$_2$O Sample. Figures 4E, 5E, 6E, and 7E describe the temperature dependence of the ν_{OH} band of this sample and of its spectral parameters.

Similar to the 3:1 Ar/H$_2$O sample, two bands were found in the free OH region, at 3720 cm^{-1} and 3704 cm^{-1}. The assignment of these bands to small H$_2$O clusters is again preferred over that to dangling OH bonds: already with the beginning of external neon evaporation at 9.5 K, their integrated intensity decreases by 50% and at 40 K only remnants (<10%) were found.

While holding the sample at 9.5 K and letting neon evaporation to continue, the baseline develops the Christiansen filter

effect:[46-49] transmittance on the high-frequency side of the ν_{OH} band is enhanced as compared to the lower frequency side. Previous studies[50,51] noted reflections of Ic and Ih ices at 3230 and 3130 cm^{-1}, attributed to either crystalline solids or to polycrystalline powders, unlikely to exist in the clusterlike, amorphous sample formed here. The Christiansen effect implies that the refractive index of the sample approaches $n = 1$ in this frequency range. While the infrared $n(\lambda)$ values for amorphous ice are of 1.25−1.3,[5,52] Berland et al.,[5] showed that a decrease in n values reflects a parallel decrease in density. The sample, from which Ne evaporates, develops a large number of internal voids, reducing its density value to below 0.94 g/cm^3 of "low-density" amorphous ice, with a corresponding decrease in $n(\lambda)$. In a previous study[27] this sample was shown to possess, after the temperature cycling, a high degree of bulk porosity and was easily penetrated by a significant amount of CO, while its argon counterpart (the previously discussed sample) demonstrated essentially surface effects. Thus our results are in accordance with Mayer et al., who suggested[8] the existence of several small clusters along with a large one, creating a number of solid areas demonstrating different homogeneity and infrared spectral features.

At a temperature of 5 K the band could be fitted by four components at 3564, 3470, 3344, and 3175 cm^{-1} with relative integrated absorptions ratios of 1:6:21:10. At 9.5 K, this changes to 1:27:33:21, due to a decreasing intensity of the high-frequency component and an enhancement of the 3470 and 3175 cm^{-1} bands. At about 11 K the 3560 cm^{-1} constituent disappeared, leaving a three-component feature of 3390, 3270, and 3174 cm^{-1} peak frequencies. This elimination of the 3550 cm^{-1} part is further evidence that the released neon comes in part from the sample interior.

At about 30 K, a second system pressure increase occurs, caused here solely by the evaporation of internally trapped neon. This is in accord with a previous mass spectrometric study of a solid neon/ice mixture,[17] even though the latter describes a much more rugged, fluffy, even hairlike, ice sample. The similitude of neon evaporation temperatures in both studies, along with the results for the four samples discussed above, point to 30 K as being the temperature for the first important stage of amorphous ice annealing.

The $\nu_{OH}(T)$ curve (Figure 5E) shows an overall decrease of the band frequency with temperature, characteristic of the slow H-bonding strengthening upon annealing, with two obvious steps at 10 and 30 K, as expected.

$\Delta\nu_{1/2}(T)$ (Figure 6E) shows a slight increase at very low temperatures, followed by a sharp increase at 11 K, revealing disorder induced by the neon evaporization. At higher temperatures, however, the bandwidth gradually decreases, with a steeper decrease at the 30 K temperature region, the first ice annealing stage.

The integrated absorption, $A(T)$ (Figure 7E), also demonstrates a steep rise at 10 K, as well as a slight maximum at 30 K. The curve does not indicate, at any stage, a loss of part of the ice with the evaporating neon, as was noted for argon.

The rather narrow ν_2 band peaks at 1639 cm^{-1}, with a shoulder at 1680 cm^{-1}, similar to the film of the 3:1 Ar/H$_2$O mixture. Warming shifts the band positions closer to those of pure ice and broadens it due to the growth of the 1680 cm^{-1} shoulder. The ν_R region shows a behavior similar to the analogous 3:1 argon/H$_2$O mixture. The band narrows and its peak blue-shifts upon warming from 745 cm^{-1} (5 K) to 815 cm^{-1} (50 K). These temperature affected changes may also be responsible for changes in the ν_2 bending mode region by a coupling of the latter with the $2\nu_R$ overtone.
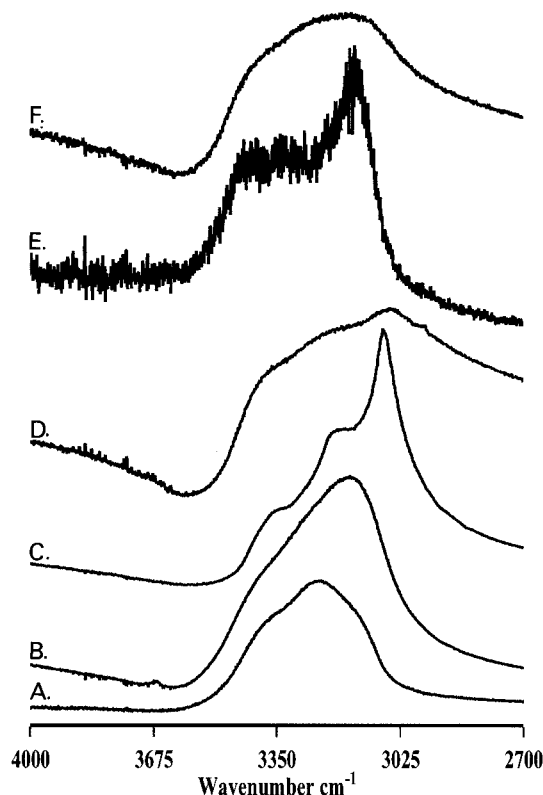
Figure 10. Effect of thermal release of argon and neon on the "3 μm" ice infrared band. (A) Pure ice as deposited at 5 K on a CsI window. (B) 4:1 Ne/H_2O sample as deposited at 5 K on a CsI window. (C) Sample B annealed to 165 K and recooled to 5 K. (D) 4:1 Ne/H_2O sample, deposited at 5 K, after fast warming to 11 K and recooling to 5 K. (E) Pure ice, deposited on an argon layer at 5 K, after fast warming to 39 K and recooling to 5 K. (F) Pure ice, deposited on an argon layer at 5 K, after fast warming to 45 K, and recooling to 5 K.

Thermal release of the neon from a concentrated 4:1 Ne/H_2O layer was shown[27] to produce an ice which can absorb a significant amount of deposited CO, which is in turn ejected completely only upon crystalization at about 165 K. The annealing process of this mixed film (section A5) resulted in a ν_{OH} band peaking at 3140 cm^{-1}, with a shoulder at about 3400 cm^{-1}. This spectrum is very different from the three component pure ice spectrum discussed in A1 (Figure 10A,B). Higher temperatures did not change the band nature and only at 165 K, where crystallization is expected, it narrows (Figure 10C) revealing three components at 3380, 3200, and 3066 cm^{-1}. The baseline distortion (Christiansen effect) attributed to structural changes and density decrease when the initial neon quantity is released persists to the highest temperatures checked. The ν_{OH} of this crystallized sample differs considerably from the analogous Ic or Ih bands,[7,27] especially by the presence and relative intensity of the low-frequency 3066 cm^{-1} band component.

Bulk porosity is thus reflected in the enhancement of the lowest frequency component of $(H_2O)_{as}$, a component completely absent for small H_2O clusters. This porosity is produced by the fast gas release which forms new vacancies and thus decreases the overall solid density, at same time compresses the remaining ice, decreases the O–O distances and red-shifts its ν_{OH} band. Experiments in which argon and neon were rapidly ejected from solid mixtures with H_2O, or from layers beneath a pure ice sample confirm this assumption. In all these experiments the ice solid was visibly cracked, ejected in part with the released rare gas and sometimes even peeled off the cold tip. The ν_{OH} bands of three such experiments, given in

Figure 10D–F, show maxima at 3050, 3140, and 3120 cm^{-1}, respectively. In these solids the formation of almost macroscopic voids is clear-cut and always accompanied by the enhancement of the low-frequency component of ν_{OH}. As the cracks and voids are formed by the rare-gas release, it is naturally the Ar–H_2O or Ne–H_2O bonds that are broken, rather than H-bonds within the solid H_2O.

The argument above is also the reason that these cracked, hollow, low-density ices do not show spectroscopically new free, dangling OH bonds due to gas release but constitute a very strained, metastable solid ready to absorb small chemical species inside its voids. The spectra of this bulk porous ice show a remarkable resemblance to that of vitrified liquid water[28] from supercooled aqueous aerosol droplets. The OH band of the latter has the strongest peak at 3115 cm^{-1}, and the spectrum shows a distinct Christiansen effect, which could be diminished by covering the sample with an argon layer. As the Christiansen effect is associated with structural and density changes reflected in the refractive index, its prominence in vitrified glasses and in our bulk porous ice implies a basic difference between them and vapor-deposited solid ice. The spectral similarity between supercooled water ice[28] and our porous ice is quite reasonable in view of the strains introduced in the latter during the internal gas release process. Such similarity between annealed amorphous ice and "hyperquenched glassy water" was also found on the basis of calorimetric studies.[29]

(6) Annealing of an Ice from a 10:1 CO/ H_2O Premixed Sample. The ice produced from a 10:1 CO/H_2O mixture freezes with an external CO solid layer,[15,27] shown to evaporate at 30–40 K.[27] Annealing effects are reproduced in the spectra of Figure 4F and in the graphs of Figures 5F, 6F, and 7F.

The relatively narrow (318 cm^{-1}) ν_{OH} band (Figure 4F) peaking at 3300 cm^{-1} at 5 K red-shifts to 3275 cm^{-1} at 50 K, a much smaller shift of only 25 cm^{-1} than observed for the other mixed ices warmed to this temperature. Up to about 50 K, the rather symmetric band is composed of three components at 3220, 3300, and 3400 cm^{-1}, attributed by Whalley[35] to ν_3 + TO, ν_3 + LO, and ν_1 out-of-phase vibrations. Only at higher temperatures, the pure ice band structure 3400, 3250, and 3170 cm^{-1} is revealed. As demonstrated above, the development of the 3170 cm^{-1} (ν_1 in-phase mode band[35]) points to a more ordered, strongly H-bonded solid. Thus ice solidification around CO cluster grains delays but does not prevent completely the crystallization stage, achieved by pure water vapors already at 5 K, to temperatures at which this internally frozen CO starts to evaporate.

Both the $\nu_{OH}(T)$ and $\Delta\nu_{1/2}(T)$ curves (Figures 5F and 6F) show a monotonous decrease, indicating H-bonding strengthening with a small maximum at 45 K, when the release of internal CO starts. At this temperature, the $A(T)$ curve (Figure 6F) also has a prominent maximum. Due to the external CO release (30–40 K), the annealing stage, observed for other ices at around 30 K, cannot be clearly discerned here.

The ν_2 band (1657 cm^{-1} at 5 K) is rather symmetrical with a width of 87 cm^{-1}, which blue-shifts (1665 cm^{-1} at 55 K) and broadens with increasing temperature. The shift is expected for a more H-bonded sample, while the broadening is due to the development with temperature of a shoulder at 1550 cm^{-1}, similar to the pure ice on a CsI substrate.

The ν_R band shows a slow monotonous increase with temperature of the peak frequency, accompanied by band narrowing, thus more resembling the pure ice deposited on CsI, than the mixed ice samples. In all, the spectral observations support the contention of the rather crystalline nature of this ice layer.

Pure and Mixed Amorphous Ice Samples

J. Phys. Chem. B, Vol. 101, No. 43, 1997 **8705**

(7) Annealing Effect on the High-Frequency OH Stretching Bands. As noted above, the 3720 and 3704 cm^{-1} lines of the Ne/H_2O as well as the doublet of the Ar/H_2O sample at the same frequencies (Table 1) are assigned by us to small H_2O clusters rather than to OH bonds dangling from ice microporous surface.[20] Upon warming to about 10 K, when neon release begins, the higher frequency, 3720 cm^{-1}, remains almost constant, whereas the lower frequency one irreversibly red-shifts from 3704 to 3695 cm^{-1}. The 3720 cm^{-1} bandwidth irreversibly increases and its intensity becomes too small to provide valuable data, whereas the more intense 3704 cm^{-1} line first shows an increase in width up to 10 K and then a monotonous decrease, both changes being irreversible. Such behavior is also shown by the 3704 cm^{-1} of the Ar/H_2O sample up to 40 K. The sameness of frequencies in both mixed ice layers, their temperature dependence, and their almost complete disappearance at about 40 K support their present assignment.

The band broadening with rising temperature supports our attribution of the 3704 and 3720 cm^{-1} doublet to small water clusters, as it is taken to reflect mode coupling.[10] This broadening may be contrasted with the thermal behavior of the decoupled OH oscillator of HDO/H_2O polycrystalline ice[36] where ν_{OH} increases slowly with temperature due to thermal expansion, but the width is practically temperature independent. A more specific assignment, also in line with their different thermal behavior, would be of the lower frequency band to 3-coordinated water molecules in these clusters and of the higher frequency one to 2-coordinated species.

B. Cluster Size Considerations. A classification of the ice bands discussed would be to attribute the 3390, 3234, 3140, 1653, 1550, and 800 cm^{-1} bands to the more crystalline $(H_2O)_{as}$, and the 3720, 3704, 3550, 3450, 1660–1680, 1635, 850, and 650 cm^{-1} spectral features to smaller, less ordered and more clusterlike species. In the following we shall relate the properties of the latter bands to cluster size considerations.

In a 400:1 argon/H_2O deposition at 5 K (Figure 11A), monomeric and dimeric bands were recorded, the lowest frequency in the OH stretch region being at 3574 cm^{-1}, a dimeric[34,53,54] feature. Increasing H_2O ratio four times, reveals a very weak band at 3520 cm^{-1}, close to the frequency attributed[34,55] to $(H_2O)_3$ cyclic trimer (Figure 11B). At higher deposition temperatures (10 and 15 K), this band gains intensity and gets broader ($\Delta\nu_{1/2} = 20$ cm^{-1}), and in a 20 K deposition it broadens further (50 cm^{-1}) and three additional broad bands appear: a strong doublet at 3380, 3320 cm^{-1} (($\Delta\nu_{1/2}$ about 100 cm^{-1}), and a very weak line at 3230 cm^{-1} (Figure 11C), with no monomer bands being observed. Temperature cycling to 35 K of a 100:1 Ar/H_2O sample deposited at 5 K yields similar results. Assuming diffusion in the matrix, the 3520, 3380, and 3230 cm^{-1} features may be assigned to three different $(H_2O)_n$ polymers, of increasing n, respectively. The width of the 3520 cm^{-1} band precludes its assignment to simple trimers, and, on the other hand, the 3140 cm^{-1} band of solid ice does not emerge at this stage. Taking the assignment by Whalley[35] of the latter to the in phase ν_1 mode of a cluster of at least 25 molecules, we use this value as an upper limit for this polymer size.

The intensity distribution in the coupled OH band of the $(H_2O)_{19}$ cluster,[54,56] where the 3250 cm^{-1} component is stronger than the 3550 cm^{-1} one, is significantly different from that in Figure 10C. Our band resembles more closely their $(H_2O)_6$ band. The energetically favorable hexamer structure was described as a stack of two three membered rings and such trimeric rings were also found in structurally less stable polymers.[57] Thus, the persisting and broadening of the 3500–3600 cm^{-1} absorption in the warmed samples may indicate that
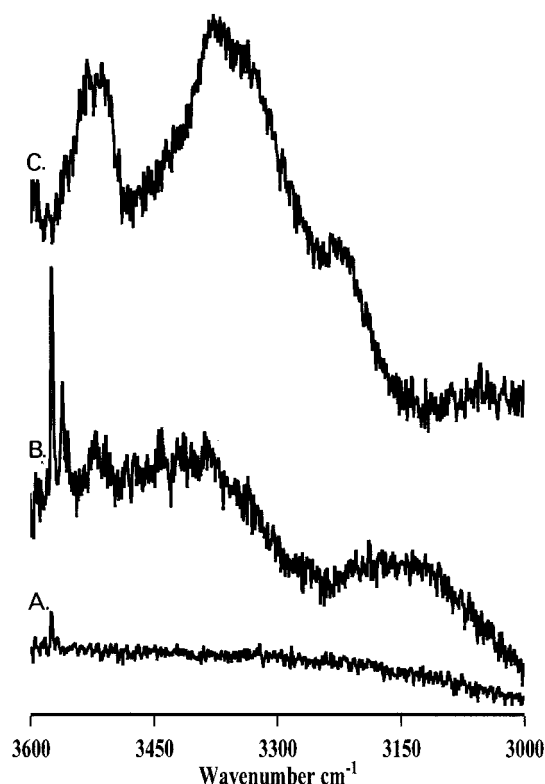
Figure 11. Concentration and deposition temperature effects on the ν_{OH} frequency region of argon/H_2O samples. (A) 400:1 Ar/H_2O sample as deposited at 5 K. (B) 100:1 Ar/H_2O sample as deposited at 10 K, cooled to 5 K. (C) 100:1 Ar/H_2O sample as deposited at 20 K, cooled to 5 K.

the first appearance of the weak 3520 cm^{-1} band corresponds to the formation of H_2O trimers, but as warming continues, these stable cyclic trimer units are also building units in higher polymers. We, therefore, estimate that the coupled OH spectrum demonstrated of Figure 10C, together with the 3704 cm^{-1} band, belong essentially to $(H_2O)_n$ clusters of $n < 10$. We note that the features attributed to the trimer/hexamer units disappear at the phase transition to crystalline Ic ice. In the more concentrated 2.5:1 and 3:1 Ar/H_2O the OH stretching mode band becomes very similar to the $(H_2O)_{19}$ absorption.[54,56]

Summary

The major conclusions of the above discussion of laboratory produced ice layers, which are intended to bear similarities with stratospheric or interstellar ice particles, are as follows:

The spectroscopic parameters, band peak wavenumber positions, bandwidths, and integrated intensities, especially those of the coupled and decoupled OH stretching mode bands, are very sensitive to structural modifications in the solid ice layers. Abrupt changes in the temperature-dependent curves of these parameters signify processes such as annealing, morphological changes, phase transitions, internal and adsorbed gas release, and ice grain ejection. It was shown that $(H_2O)_{as}$ annealing is a gradual process taking place even at very low temperatures and that 30 K is an important stage in the crystallization of amorphous ice itself, while 10, 24, and 42 K are the gas release temperatures of neon (the two former) and argon from mixed solids.

The formation of internal cracks and voids in the amorphous ice by fast release of rare-gas species from mixed ice solids is reflected in the infrared spectrum in the enhancement of the lowest frequency (3150 cm^{-1}) component of the ν_{OH} transition. An infrared spectroscopic similarity exists between the bulk

porous ice formed by rare gas release and supercooled water solid and both differ significantly from the usual vapor deposited amorphous ices.

References and Notes

(1) Hagen, W.; Tielens, A. G. G. M.; Greenberg J. M. *Astron. Astrophys.* **1983**, *117*, 132.

(2) Leger, L.; Gauthier, S.; Defourneau, D.; Rouan, D. *Astron. Astrophys.* **1983**, *117*, 164.

(3) Smith, R. G.; Sellgren, K.; Tokunaga, A. T. *Astrophys. J.* **1988**, *334*, 209.

(4) Schutte, W. A.; Greenberg J. M. *Astron. Astrophys.* **1991**, *244*, 190.

(5) Berland, B. S.; Brown, D. E.; Tolbert, M. A.; George, S. M. *Geophys. Res. Lett.* **1995**, *22*, 3493.

(6) Dowell, L. G.; Rinfret A. P. *Nature* **1960**, 188, 1144.

(7) Hagen, W.; Tielens, A. G. G. M.; Greenberg, J. M. *Chem. Phys.* **1981**, *56*, 367.

(8) Mayer, E.; Pletzer R. *J. Chem. Phys.* **1984**, *80*, 2939.

(9) Narten, A. H.; Venkatesh, C. G.; Rice, S. A. *J. Chem. Phys.* **1976**, *64*, 1106.

(10) Sivakumar, T. C.; Schuh, D. Sceats M. G.; Rice S. A. *J. Chem. Phys.* **1978**, *69*, 3477.

(11) Ghormley, J. A. *J. Chem. Phys.* **1967**, *46*, 1321.

(12) Adamson, A. W.; Dormant, L. M.; Orem M. *J. Colloid Interface Sci.* **1967**, *25*, 206.

(13) Ocampo, J.; Klinger J. *J. Colloid Interface Sci.* **1982**, *86*, 377.

(14) Pletzer R.; Mayer E. *Nature* **1986**, *319*, 298.

(15) Kouchi, A. *J. Cryst. Growth* **1990**, *99*, 1220.

(16) Laufer, D.; Kochavi, E.; Bar-Nun, A. *Phys. Rev. B* **1987**, *36*, 9219.

(17) Bar-Nun, A.; Dror, J.; Kochavi, E.; Laufer, D. *Phys. Rev. B* **1987**, *35*, 2427.

(18) Zhang, Q.; Buch V. *J. Chem. Phys.* **1990**, *92*, 1512.

(19) Zhang, Q.; Buch V. *J. Chem. Phys.* **1990**, *92*, 5004.

(20) Buch, V.; Devlin, J. P. *J. Chem. Phys.* **1991** *94*, 4091.

(21) Devlin, J. P.; Silva, S. C.; Rowland, B.; Buch, V. In *Hydrogen Bond Network*; Bellissent-Funel M.-C., Dore, J. C., Eds.; Kluwer Academic Publishers: 1994; p 373.

(22) Rowland, B.; Devlin, J. P. *J. Chem. Phys.* **1991**, *94*, 812.

(23) Rowland, B.; Fisher, M.; Devlin, J. P. *J. Chem. Phys.* **1995**, *95*, 1378.

(24) Devlin, J. P. *J. Phys. Chem.* **1992**, *96*, 6185.

(25) Rowland, B.; Fisher M.; Devlin, J. P. *J. Phys. Chem.* **1993**, *97*, 2485.

(26) Hessinger J.; Pohl, R. O. *J. Non-Cryst. Solids* **1996**, *208*, 151.

(27) Givan, A.; Loewenschuss, A.; Nielsen, C. J. *Vib. Spectrosc.* **1996**, *12*, 1.

(28) Mayer E. *J. Phys. Chem.* **1985**, *89*, 3474.

(29) Hallbruker, A.; Mayer E.; Johari, G. P. *J. Phys. Chem.* **1989**, *93*, 4986.

(30) Hardin A. H.; Harvey, K. B. *Spectrochim. Acta* **1972**, *29A*, 1139.

(31) Ritzhaupt, G.; Smirl N.; Devlin, J. P. *J. Chem. Phys.* **1976**, *64*, 435.

(32) Eisenberg, D.; Kautzmann, W. *The Structure and Properties of Water*; Oxford University Press: Oxford, 1969.

(33) Kittel, C. *Introduction to Solid State Physics*, 6th ed.; J. Wiley and Sons Inc.: New York, 1986; p 55.

(34) Givan, A.; Loewenschuss, A.; Nielsen, C. J. *J. Chem. Soc., Faraday Trans.* **1996**, *92*, 4927.

(35) Whalley, E. *Can. J. Chem.* **1977**, *55*, 3429.

(36) Sivakumar, T. C.; Schuh, D.; Sceats, M. G.; Rice S. A. *Chem. Phys. Lett.* **1977**, *48*, 212.

(37) Bergren, M. S.; Schuh, D.; Sceats, M. G.; Rice, S. A. *J. Chem. Phys.* **1978**, *69*, 3477.

(38) Klein, M. L.; Venables, J. A. In *Rare Gas Solids*; Academic Press Inc.: London, 1976; p 885.

(39) Apfelbaum, F.; Mayer, I.; Lebugle, A. *J. Cryst. Growth* **1994**, *144*, 304.

(40) Galeener, F. L.; Lukovski G. *Phys. Rev. Lett.* **1976**, *37*, 1474.

(41) Venkatesh, C. G.; Rice, S. A.; Bates, J. B. *J. Chem. Phys.* **1975**, *63*, 1065.

(42) Loewen, H. W.; Jodl, H. J.; Loewenschuss, A.; Daeufer, H. *Can. J. Phys.* **1988**, *66*, 308.

(43) Brill V. R.; Tippe, A. *Acta Crystallogr.* **1967**, *23*, 343.

(44) Flubacher, D.; Leadbetter, A. J.; Morrison, J. A. *J. Chem. Phys.* **1960**, *33*, 1751.

(45) Novak, A. *Struct. Bonding* **1974**, *18*, 177.

(46) Clarke, R. H. *Appl. Opt.* **1968**, *7*, 861.

(47) Carlon, H. R. *Appl. Opt.* **1979**, *18*, 3610.

(48) Price, W. C.; Tetlow, K. S *J. Chem. Phys.* **1948**, *16*, 1157.

(49) Laufer, G.; Huenke, J. T.; Royce, B. S. H.; Teng, Y. C. *Appl. Phys. Lett.* **1980**, *37*, 517.

(50) Bertie, J. E.; Whalley, E. *J. Chem. Phys.* **1964**, *40*, 1637.

(51) Ockman, N. *Adv. Phys.* **1958**, *7*, 199.

(52) Kislovskii, L. D. *Opt. Spektrosk.* **1959**, *7*, 201.

(53) Bentwood, M.; Barnes A. G.; Orville-Thomas, W. J. *J. Mol. Spectrosc.* **1980**, *84*, 391.

(54) Vernon, M. F.; Krajnovich, D. J.; Kwok, H. S.; Lisy, J. M.; Shen, Y. R.; Lee, Y. T. *J. Chem. Phys.* **1982**, *77*, 47.

(55) Engdahl, A.; Nelander, B. *J. Chem. Phys.* **1987**, *86*, 4831.

(56) Page, R. H.; Vernon, M. F.; Shen, Y. R.; Lee, Y. T. *Chem. Phys. Lett.* **1987**, *141*, 1.

(57) Franken, K. A.; Jalaie, M.; Dykstra, C. E. *Chem. Phys. Lett.* **1992**, *198*, 59.